# SUMMARY OF RESEARCH

**for**

## A Graduate Student Research Program Entitled:
## A Novel Method for Reducing Rotor Blade-Vortex Interaction

**Prepared for**


**NATIONAL AERONAUTICS AND SPACE ADMINISTRATION**
**AMES RESEARCH CENTER**
**MOFFETT FIELD, CA 94035-1000**

**GRANT NO. NGT 2-52204**

**August 1, 1995 to July 31, 1999**


**Submitted by**


**Graduate Student: A. T. Glinka**

**Arizona State University**
**Department of Mechanical and Aerospace Engineering**
**Tempe, AZ 85284**

# The Flip-Tip Rotor Blade: A Novel Method for Reducing Helicopter Rotor Noise

A. T. Glinka
Arizona State University

Abstract

One of the major hindrances to expansion of the rotorcraft market is the high-amplitude noise they produce, especially during low-speed descent, where blade-vortex interactions frequently occur. In an attempt to reduce the noise levels caused by blade-vortex interactions, the flip-tip rotor blade concept was devised. The flip-tip rotor increases the miss distance between the shed vortices and the rotor blades, reducing BVI noise. The distance is increased by rotating an outboard portion of the rotor tip either up or down depending on the flight condition. The proposed plan for the grant consisted of a computational simulation of the rotor aerodynamics and its wake geometry to determine the effectiveness of the concept, coupled with a series of wind tunnel experiments exploring the value of the device and validating the computer model. The computational model did in fact show that the miss distance could be increased, giving a measure of the effectiveness of the flip-tip rotor. However, the wind experiments were not able to be conducted. Increased outside demand for the 7'x10' wind tunnel at NASA Ames and low priority at Ames for this project forced numerous postponements of the tests, eventually pushing the tests beyond the life of the grant. A design for the rotor blades to be tested in the wind tunnel was completed and an analysis of the strength of the model blades based on predicted loads, including dynamic forces, was done.

# Table of Contents



# List of Figures

## List of Tables

## Introduction

Police departments, emergency medical teams, and traffic reporters presently use helicopters extensively in urban areas. Although these rotorcraft provide a potentially attractive means of transportation around and between urban areas, the noise associated with their operation presents a major obstacle to community acceptance and makes deployment of a larger number of them unlikely at this time. Alternative concepts such as the tilt rotor produce lower levels of noise in forward flight, but their rotor noise level is comparable to that of conventional helicopters when operating in vertical flight mode. Rotorcraft produce sound pressure levels in excess of those now considered acceptable for urban-center operation. There is a need to make rotorcraft more publicly acceptable, and, in order to do this, rotorcraft noise levels must be reduced.

Helicopters and other rotorcraft are especially noisy during three flight regimes: high-speed forward flight, high g-force maneuvers, and low-speed descent. The reduction of noise levels during low-speed descent will be most beneficial for increased public acceptance of rotorcraft. This is because low-speed descent operation most often occurs over highly populated areas, close to the ground, while rotorcraft are landing. This noise, while landing, is a tremendous hindrance to the use of rotorcraft for city-center to city-center travel, which is considered one of the principle ways in which rotorcraft can be exploited. Currently the Civil Tilt Rotor program at NASA is exploring the possibilities of the tilt rotor to used for just such a purpose.

## Blade-Vortex Interaction Noise

The major sources of noise during low-speed descent are the pressure fluctuations arising from the interactions between a rotor blade and a wake vortex. As with conventional fixed wings, lifting rotor blades produce trailing vortex systems, varying in strength along the radius, but with the highest magnitude of vorticity near the rotor tip. Thus, the tip vortices are the most important with respect to noise because they are the strongest. Blade-vortex interactions occur as trailing tip vortices from preceding blades interact with the following blades. These interactions cause dramatic pressure changes on the blades, which translate directly into increased noise levels.

Blade-Vortex Interaction (BVI) noise levels depend most strongly on four major parameters. These include blade-vortex geometry, vortex core size, vortex strength, and vortex miss distance. Blade-vortex geometry is important because parallel interactions, where the vortex axis and the

blade are roughly parallel to each other, have a greater influence on noise levels than perpendicular or oblique interactions. During a parallel interaction, the vortex generally affects a larger fraction of the rotor blade, and the velocities it induces affect the blade pressures more adversely. Vortex core size is important because the tighter the vortex the greater the velocity it induces at close distances, thus creating larger pressure disturbances on the rotor blade. As the strength of the interacting vortex increases, so does the increase in noise levels, again because of the larger pressure disturbances induced on the rotor blade. The vortex miss distance refers to the distance between the vortex and the blade with which it interacts. A BVI noise model developed by Hardin[1] indicates that the acoustic pressure amplitude varies as the inverse of the miss distance squared, so that increasing the miss distance will greatly reduce the noise produced by the interaction.

## Controlling BVI Noise

Previously, various passive and active techniques have been used in attempts to reduce BVI noise. There has been limited success in lowering BVI noise levels using these methods, but it is proposed that an effective and relatively simple noise-reduction device remains to be evaluated.

### *Previous Attempts to Control BVI Noise*

During the 1970's various rotor tip designs were investigated to determine their feasibility for reducing blade-vortex interaction noise levels.[2] The tip designs studied include such devices as the Ogee tip, flow spoiler tip, swept-tapered tip, sub-wing tip, and end-plate tip. The tip designs purported to either increase the core size of the tip vortex or to diffuse the tip vortex. It was found that a slight reduction in noise could be achieved using these devices, but with increased required power. In addition to these tip designs, the free-tip rotor [3], intended to reduce power and vibration, showed some promise for reducing BVI noise by decreasing the tip vortex strength. This tip design, however, was not pursued beyond the study stage.

Some more recent studies have investigated the use of the BERP (British Experimental Rotor Programme) tip, the use of spoilers attached to the aft portion of the rotor blade, and using two new concepts developed at NASA Langley: the Variable Impedance/Resonance blade and the Forward Swept Planform blade. The BERP blades have highly swept tips which reduce the loading on the tip and, thus prevent a tightly bound vortex from forming. Noise reductions in low-speed descent of up to 5 dBA were found when using the BERP blades. The spoiler/blade

also reduced BVI noise, but there was a significant increase in power required and in broadband noise. The Variable Impedance/Resonance blade is intended to reduce the amplitude of the normally intense unsteady surface pressure fluctuations at the leading edge region, due to vortex interactions. The Forward Swept Planform blade should alter the interaction geometry, perhaps eliminating the particularly noisy, parallel, advancing side vortex interactions. The forward sweep would cut through vortex patterns at larger angles than normal which would reduce impulsiveness and amplitude of the BVI noise. Both of the Langley blades are currently awaiting wind tunnel testing to determine their effectiveness.

Several active methods have been proposed for alleviating the unsteadiness of the loading on a rotor blade interacting with a vortex and thus, presumably, the noise associated with it. Suggested techniques for accomplishing the desired reduction include using higher harmonic control [4][5] and individual blade control [6] to vary the blade loading, as well as using trailing-edge flaps to control the strength of the trailing tip vortex. Each of these methods has been shown to be somewhat effective. However, each of them has drawbacks which include high complexity and the need for high frequency response of the control devices.

## *Flip-Tips--A New Approach*

The greatest reduction in blade-vortex interaction noise can be achieved by increasing the distance between the rotor blade and the vortex with which it interacts. The flip-tip rotor blade concept was devised in order to take advantage of the benefits associated with increasing the miss distance.

The flip-tip rotor design consists of a rotor blade which is hinged at an outboard location such that the tip may be canted up or down in order to manipulate the trajectory and the strength of the trailing tip vortex. The cant of the tip can be adjusted by means of an internal mechanism which is controlled according to the flight conditions. Since blade-vortex interactions are generally not encountered during horizontal steady flight, it is anticipated that the tip will remain uncanted during such conditions. However during low-speed descent or other maneuvers when blade-vortex interactions are likely, the tip will be positioned according to a schedule designed to minimize the interference between the rotor and its wake. Figure 1 below shows a conceptual drawing of the flip-tip rotor concept.

It is anticipated that the device will be a passively controlled one, and it will require only a low frequency response. This will help to maintain a relative simplicity of the device and rotor system.

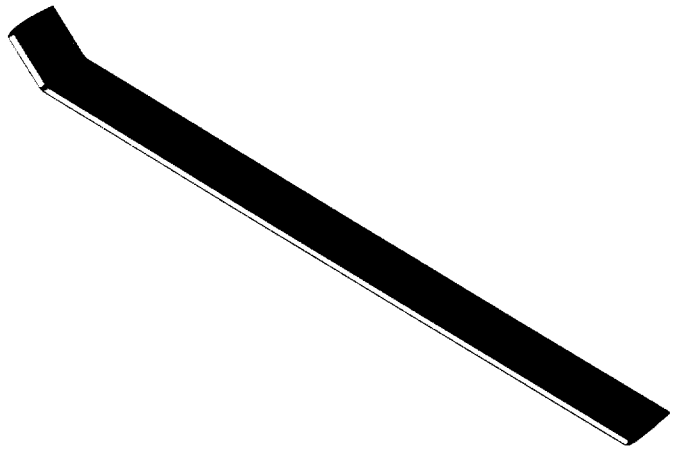

**Figure 1: The flip-tip rotor blade with a length of 10% of the rotor radius and a cant of +45 degrees.**

## Analysis

In order to study the effectiveness of the flip tips, a computer simulation of the rotor wake was needed to accurately predict the blade-vortex interaction locations. The simplest and fastest computations were desired, and yet the simulation had to provide accurate wake geometry, wake strengths, and rotor aerodynamic information. The analysis used was a free wake, vortex-lattice model. This method models the wake as a mesh of vorticity or vortex rings. The induced velocities are computed using the Biot Savart law. A full range of rotor systems can be described using this model, including both teetering and flapping rotor systems. The number of blades, the twist, the taper, and the sweep can all be varied, along with modifications in the flip-tip geometry.

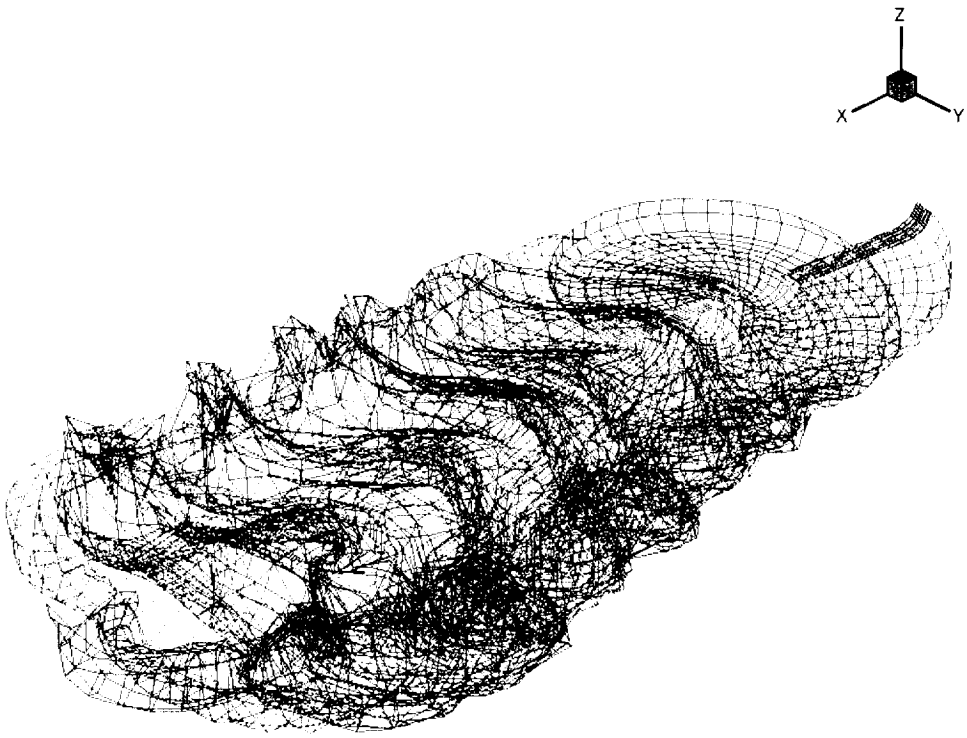


**Figure 2: The rotor free wake from a flip-tip rotor in low-speed descent.**

The rotor system initially considered is based on the AH-1/OLS rotor system. It has two blades with no twist or taper. The flight conditions studied parallel those tested in the DNW wind tunnel and reported on by the U S Army Aeroflightdynamics Directorate, ONERA, and DLR [7][8]. For the baseline case, the thrust coefficient was 0.0054. The advance ratio was 0.164 with a shaft angle of positive one degree to simulate low-speed descent flight conditions. A baseline case was run to compare the predicted BVI locations of the other three organizations. Figure 3 shows a comparison of the location of the blade-vortex interactions from the top view, while Figure 4 shows a comparison of the side view.

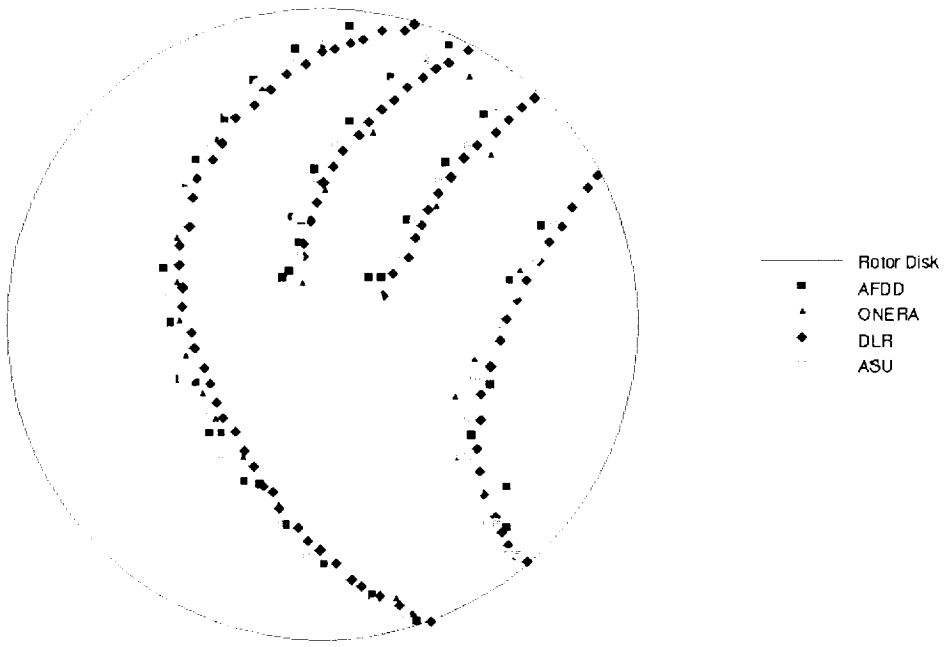


**Figure 3: A top view of the blade-vortex interactions for the baseline case compared with that of other organizations.**

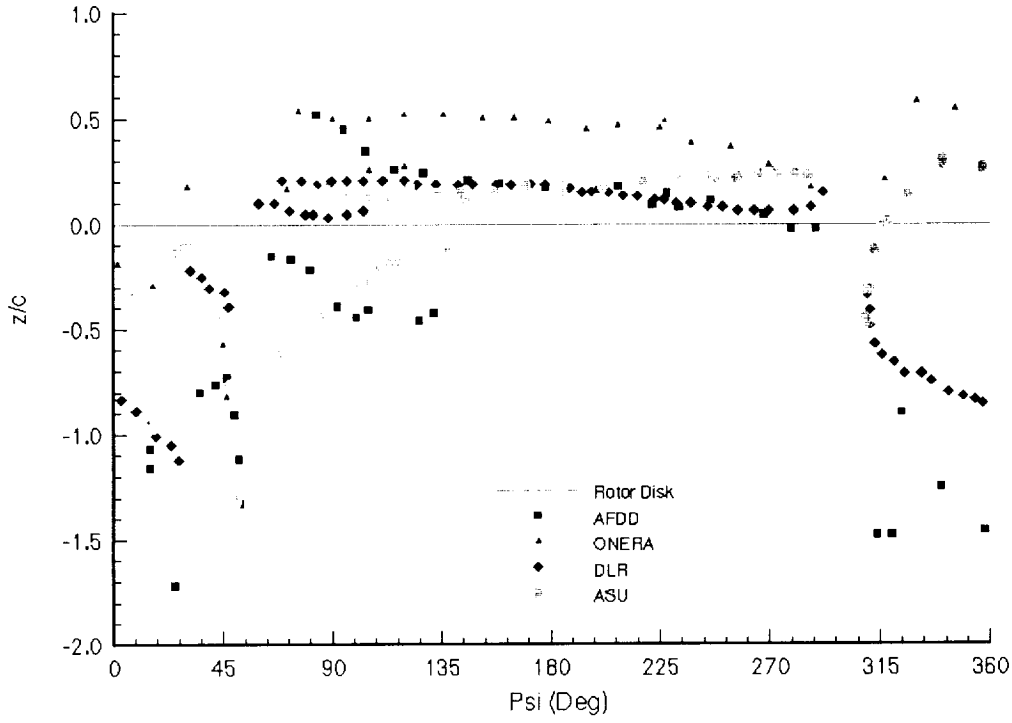


**Figure 4: A side view of the blade-vortex interactions for the baseline case compared with that of other organizations.**

Cases were run with a standard blade configuration to study the effectiveness of the flip-tips. The variation in cant angles ranged between plus and minus 60°. The flip tip length was varied from five to ten percent of the total blade radius. Figure 5 and Figure 6 show the side view of the blade-vortex interaction locations for these two flip-tip cases.

The changes in miss distance for the primary interactions were measured and are shown in Figure 7. This plot provides an indication as to which configuration of flip-tip blade would be most appropriate for the given flight conditions. The miss distances of the primary parallel interaction are plotted versus the flip-tip cant angles for two flip-tip configurations. It appears that a flip-tip length of 5% and a cant of -30 degrees, which is a minimal change in blade configuration, can provide a noise reduction of 4 times the baseline case according to the Hardin model for blade-vortex interaction noise estimation.

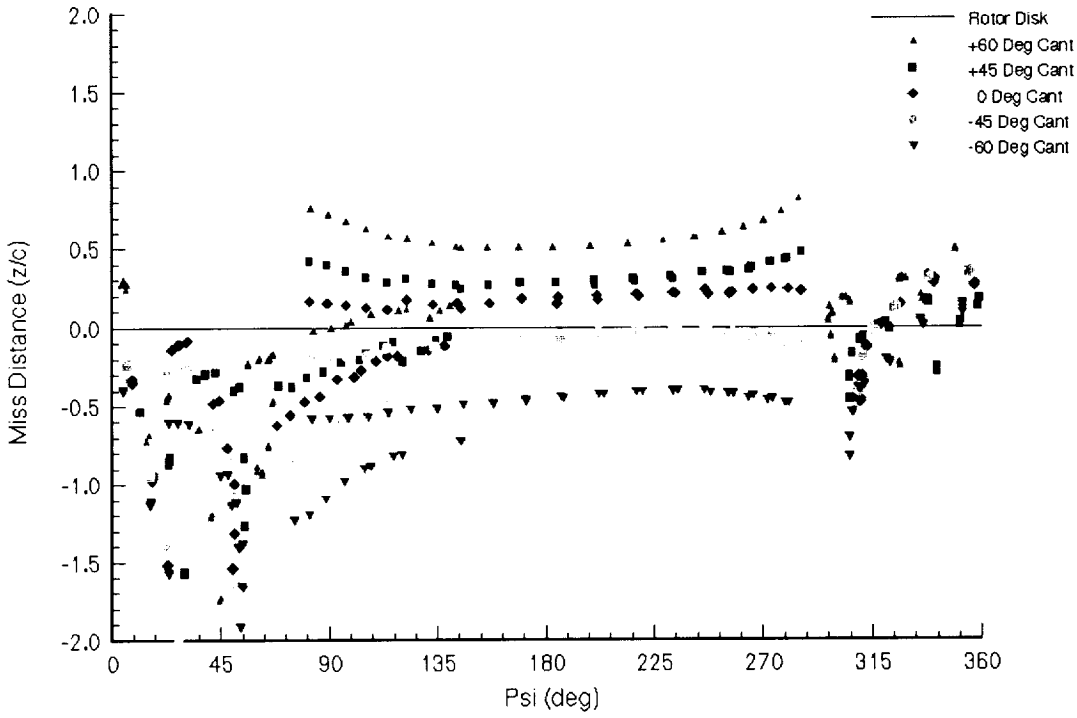


**Figure 5: Comparison of the BVI locations (side view) for the flip-tip rotor with a length of 5% of the rotor radius for various cant angles.**

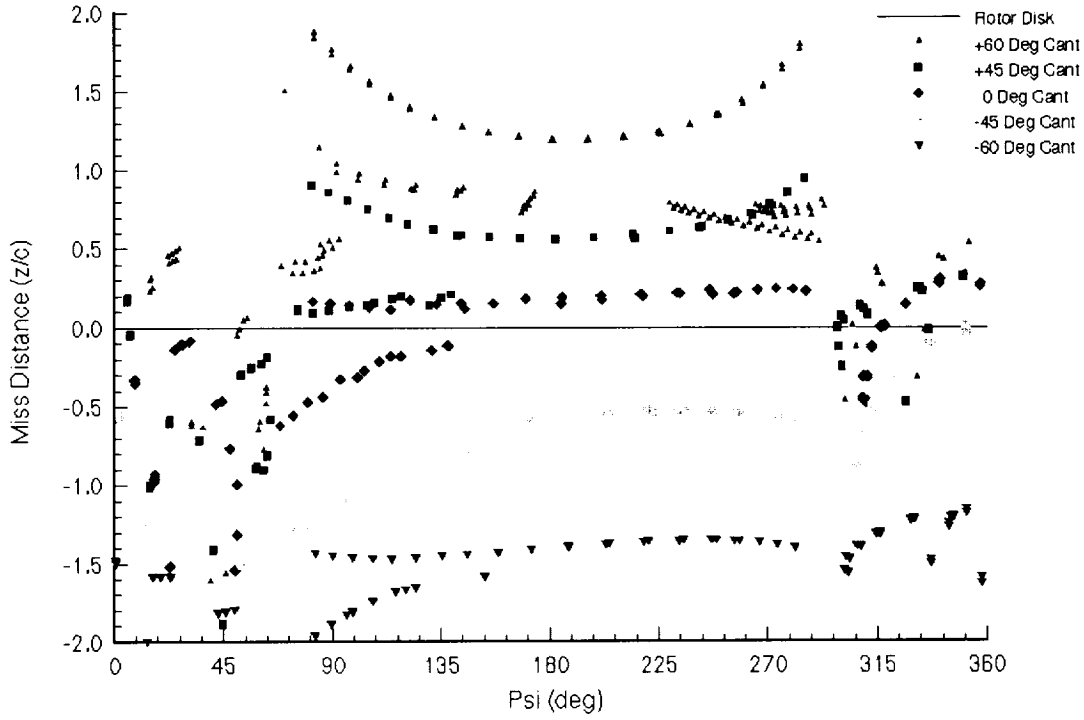


**Figure 6: Comparison of the BVI locations (side view) for the flip-tip rotor with a length of 10% of the rotor radius for various cant angles.**

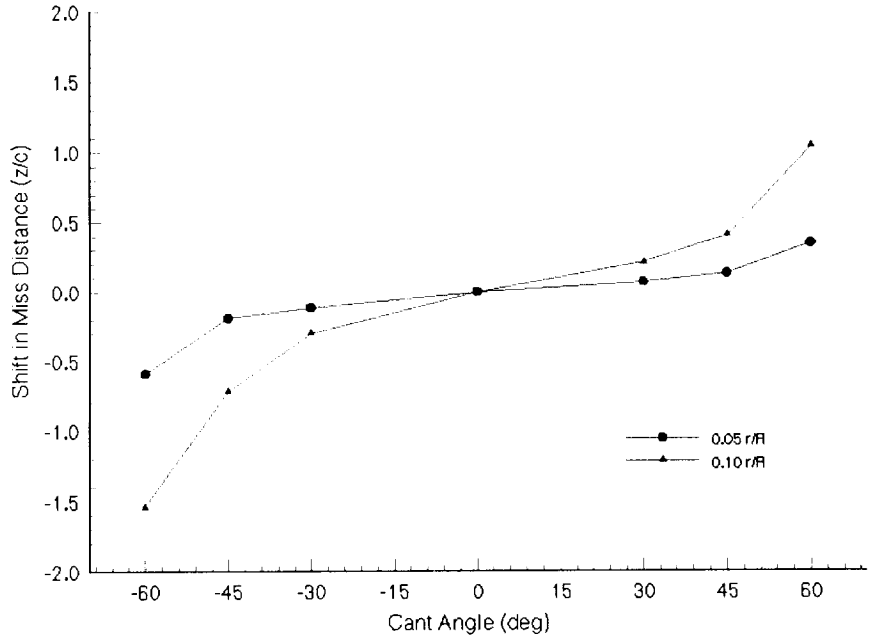


**Figure 7: Variation in the shift of the miss distance between the tip vortices of the dominant interaction and the blade.**

## Testing the Device

In order to determine the feasibility of the flip-tip rotor, experimental testing of the rotor was desired. The original test plan called for testing in both the 7'x10' wind tunnel and the 80'x120' wind tunnel at NASA Ames.

The model was first be tested in the 7'x10' wind tunnel at NASA Ames to gain a preliminary measure of the effectiveness of the rotor. In this tunnel, the ability of the device to function in actual working conditions was to be tested. The stresses on the blades, along with the required power, was to be measured for the uncanted case, the canted case, and the stages in between. In addition, a flow visualization of the wake was to be performed to determine the tip effect on the wake vortex paths.

Once the device has been shown to work, it was to be tested in the 80'x120' wind tunnel at the Ames facility. This tunnel has been acoustically treated so that noise measurements can be taken accurately. Actual noise measurements will indicate the effectiveness of the flip tip in reducing noise levels.

The goal of the original experiments was to measure the following quantities for the flip-tip rotor in all phases of its activation:

- Wake location
- Noise levels of rotor
- Blade strains/stresses
- Rotor Power
- Rotor Thrust

After further evaluation of the test plan and consultation with NASA, the experimental evaluation of the flip-tip device was modified into a two-phase process. The initial phase was to evaluate a rotor system with the blade tips permanently deflected. This was to show the effect of canted blade tips on moving the tip vortices away from the rotor plane. This testing would have been more easily accomplished than testing a variable device and would require less initial cost and complexity. Once the effectiveness of the canted blade was tested and approved, the evaluation process will move into the second phase.

The second phase of the device evaluation was to design the tip mechanism itself and its ability to cant the blade tip. The mechanism was to be designed and tested on its own. Once a working mechanism was attained, the mechanism would be incorporated into a rotor blade. This

rotor system was then to be tested and its effectiveness would be evaluated in a similar manner to the phase one blade.

One of the first hurdles encountered with the testing was the actual construction of the wind tunnel model. It soon became apparent after further discussion of matters with NASA, that the cost of the blades to be tested was significantly higher (possibly twenty times higher) than the budget of the grant allowed.

To try and reduce the cost, a local composite manufacturing company was consulted and they expressed a great desire to assist educational programs. They agreed to construct the blades, given a design and the necessary die/tool. So the tool was designed and constructed on campus. A design for the wind tunnel model was also completed and an analysis of the potential loads was performed. The construction of the blades was contingent on the wind tunnel test date.

Unfortunately, due to demand for the wind tunnel from outside sources and low priority of this test, the wind tunnel test were repeatedly postponed. Eventually, the tests were postponed past the life of the grant and subsequently the tests were then no longer scheduled. Because of this postponement the blades themselves were never constructed.

## Wind Tunnel Model

### *Airfoil/Blade Properties*

The airfoil/blade portion of the rotor is 30 inches long with a chord of 3.03 inches. and airfoil section of the blade is the NACA 0015 section. The blade will be constructed of Fiberite 948A1 composite laminate. Five plies will be used giving a wall thickness of 0.05 in. It is a cross-ply laminate and all plies will be placed in the 0°-90° direction relative to the blade axes. This composite laminate contains carbon fiber reinforced 8 harness satin fabric. A layer of an aramid composite (Kevlar) will be applied as a coating on the blade to provide both additional strength and additional safety (with its energy dissipating properties) in the event of blade failure.

There will be a spar constructed of 4130 Steel running a length of 26 inches from the hub attachment. The spar fills the nose of the blade up to the 1/4 chord of the airfoil. This spar adds both strength as well as a forward mass to stabilize the blade.

The airfoil portion of the blade will be constructed in two halves (upper surface and lower surface) which will be bonded together over the hub/blade attachment and then coated with the layer of aramid composite laminate.

Table 1 below shows the mass/area properties of the blade section while Figure 8 shows the cross section of the blade. All measurements assume that the origin is located at the leading edge of the airfoil section (1/4 chord located at 0.75 inches). Table 2 displays some of the structural properties of the composite laminate.

| | |
|---|---|
| Thickness of Skin: | 0.05 in |
| Skin Area: | 0.2921815 $in^2$ |
| Skin Perimeter: | 11.67626 in |
| Skin Bounding box: | X: 0 -- 3.027108 in |
| | Y: -0.225065 -- 0.225065 in |
| Spar Area: | 0.1813349 $in^2$ |
| Spar Bounding box: | X: 0.05 -- 0.75 in |
| | Y: -0.172665 -- 0.172665 in |
| Centroid of Skin: | X: 1.429618 in |
| | Y: 0 in |
| Centroid of Spar: | X: 0.4592923 in |
| | Y: 0 in |
| Total Centroid: | X: 0.702 in |
| | Y: 0 in |
| Skin Prin. Mom of Inertia: | X: 0.006318957 $in^4$ |
| | Y: 0.2061957 $in^4$ |
| Skin Radii of gyration: | X: 0.1470606 in |
| | Y: 1.658167 in |
| Spar Prin. Mom of Inertia: | X: 0.001280372 $in^4$ |
| | Y: 0.006085921 $in^4$ |
| Total Product of Inertia: | XY: 0.00 $in^4$ |
| Total Blade E*I | X: 94,000 lb-$in^2$ |
| | Y: 2,032,253 lb-$in^2$ |

**Table 1: Blade mass/area properties**

**Figure 8: NACA 0015 airfoil section.**

| | |
|---|---|
| 0° Tensile Strength | 90-105 ksi |
| 0° Tensile Modulus | 9-10 Msi |
| 0° Compressive Strength | 80-90 ksi |
| 0° Compressive Modulus | 9-10 Msi |
| Interlaminar Shear Strength | 9-11 ksi |

**Table 2: Composite laminate structural properties at room temperature.**

## *Hub/Blade Attachment Properties*

The hub/blade attachment portion of the blade was based on the attachment used with the LOTUS blade. It is will be constructed of both Steel and Aluminum with Steel plates giving additional support at the location of the bolt hole for attachment to the rotor stand.

There are two parts (one constructed of steel, the other aluminum) that will be bolted together to make the attachment. The steel portion forms the front quarter of the attachment and is used as a spar for the blade structure. It runs nearly the entire length of the blade. The aluminum part only runs 10 inches into the blade and provides added surface area to bond the composite skin to the attachment. Figure 9 shows a top view of the attachment, where the steel section is at the bottom of the figure and the aluminum section is at the top.

**Figure 9: Top-view of hub/blade attachment.**

When connected, the attachment can be looked at as having two main section, an exterior portion which connects to the hub and an interior portion which connects to the blade.

The first is the portion which will connect with the hub. Its dimensions correspond exactly to the dimensions of the matching part of the LOTUS blades. The hub portion of the attachment is 4.1 in. long and 2.75 in. wide as is the attachment for the LOTUS blade.

The other portion of the attachment will be the portion connected to the airfoil section of the blade. The airfoil portion of the blade will be bonded around this outer portion of the attachment to connect the two pieces together. It will be completely covered by the airfoil part and its cross section matches the shape of the inside of the airfoil portion of the blade.

There will be some form of filleting between the two sections to reduce the amount of stress concentration where they meet.

Some drawings of the attachment are presented below. The figures are not drawn to scale **with respect to each other**, but are presented to give a visual representation of the attachment. Figure 10 shows a front view of the attachment, with the part of the outboard (or portion to covered by the airfoil) cut off. Figure 11 shows a side view.

**Figure 10: Front-view of hub/blade attachment.**

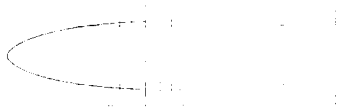

**Figure 11: Side-view of hub/blade attachment (cross-sectional view).**

## *Bonding*

As mentioned previously, the airfoil portion with be constructed in halves and these two parts will be bonded together around the hub/blade attachment. The hub/blade attachment portion and the airfoil portion of the blade will be connected using an adhesive designed especially for bonding composites to metals. It has a shear strength of 4 ksi, and given a surface area for bonding in excess of 30 $in^2$, the outer portion of the blade would not be pulled off with a CF load of less than 120,000 lbs. Once, the three pieces are bonded together, a layer of aramid composite will coat the airfoil section of the blade.

Figure 12, below, shows the blade after the two pieces have been bonded. Figure 13 shows a close up of the hub/blade attachment area. Figure 14 shows a side view.

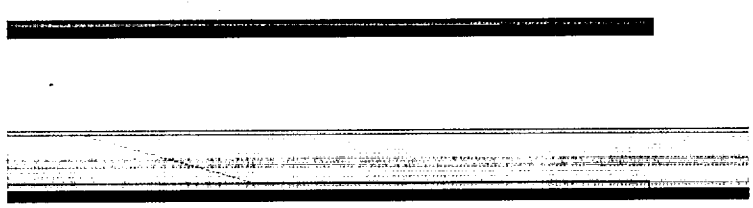

**Figure 12: Top-view of hub attachment (top) and entire rotor blade (bottom).**

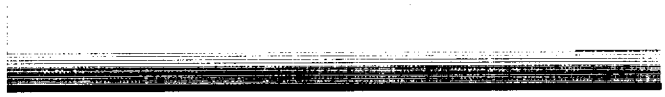

**Figure 13: Top-view of hub/blade attachment.**

**Figure 14: Side-view of hub/blade attachment with airfoil.**

## *Load Analysis*

The data presented here mirrors the format presented for the LOTUS test. The loads for the baseline Flip-Tip Rotor blade were determined using CAMRAD/JA. These results are for the original blade design (pre-steel spar) and while the interior of the blade has been changed (strengthened), the loads should be very similar, since the outer size and shape has remained the same.

The input CAMRAD operational conditions are:

| | | | | | |
|---|---|---|---|---|---|
| Velocity (kts) | = | 32.45 | RPM | = | 994.13 |
| V/(ΩR) | = | 0.164 | Tip Speed (fps) | = | 334 |
| Velocity (fps) | = | 54.78 | Tip Mach # | = | 0.2992 |
| CT | = | 0.0054 | Alpha (deg) | = | +1 |

Notes:

The blade attaches to the hub at 0.2 r/R.
The resulting forces and moments are presented in Figure 15 - Figure 21.
The loads are presented in tabular form in Appendix A.

The factors of safety were calculated from the Tsai-Hill Failure Criterion (Figure 22). As expected the FS is much larger than determined from the previous static load calculations and should be much more than adequate for the testing, in which a factor of safety of at least five was desirable.

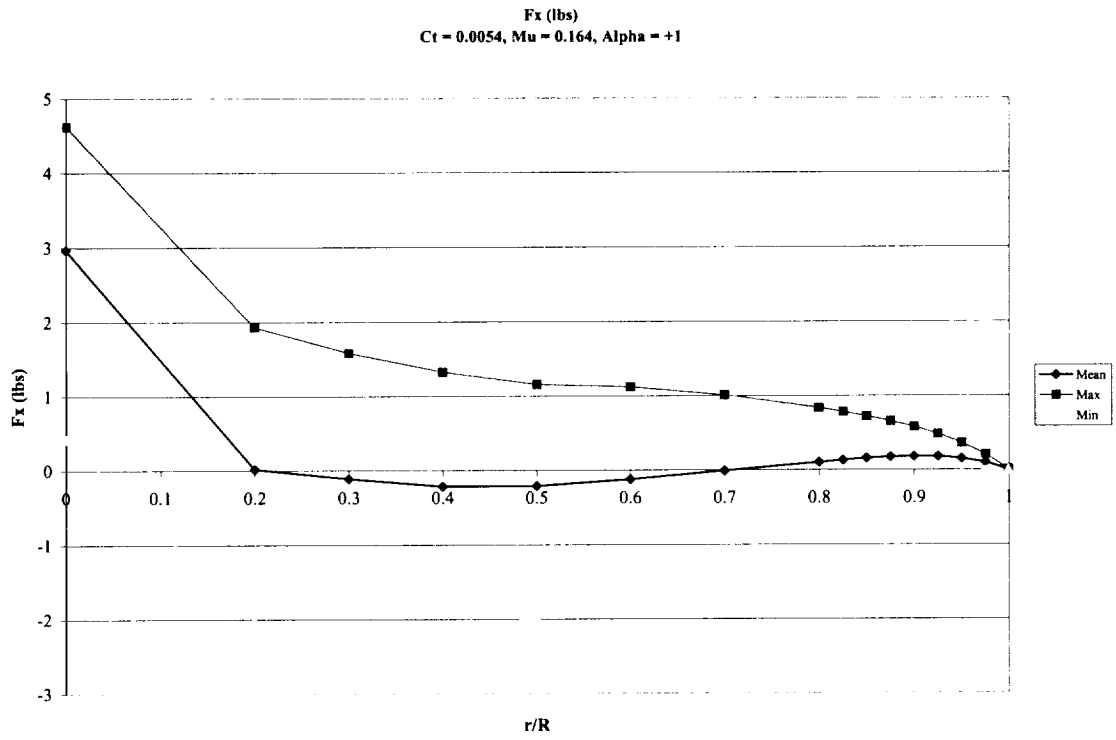


**Figure 15: Fx vs r/R**

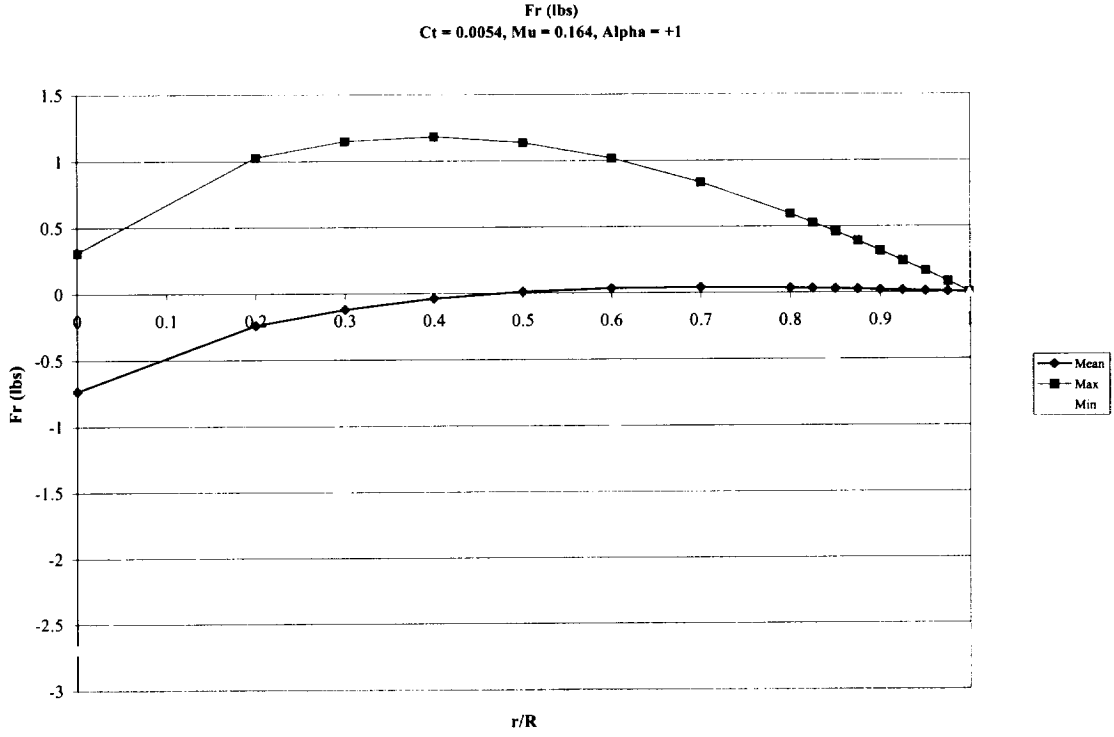


**Figure 16: Fr vs. R/R**

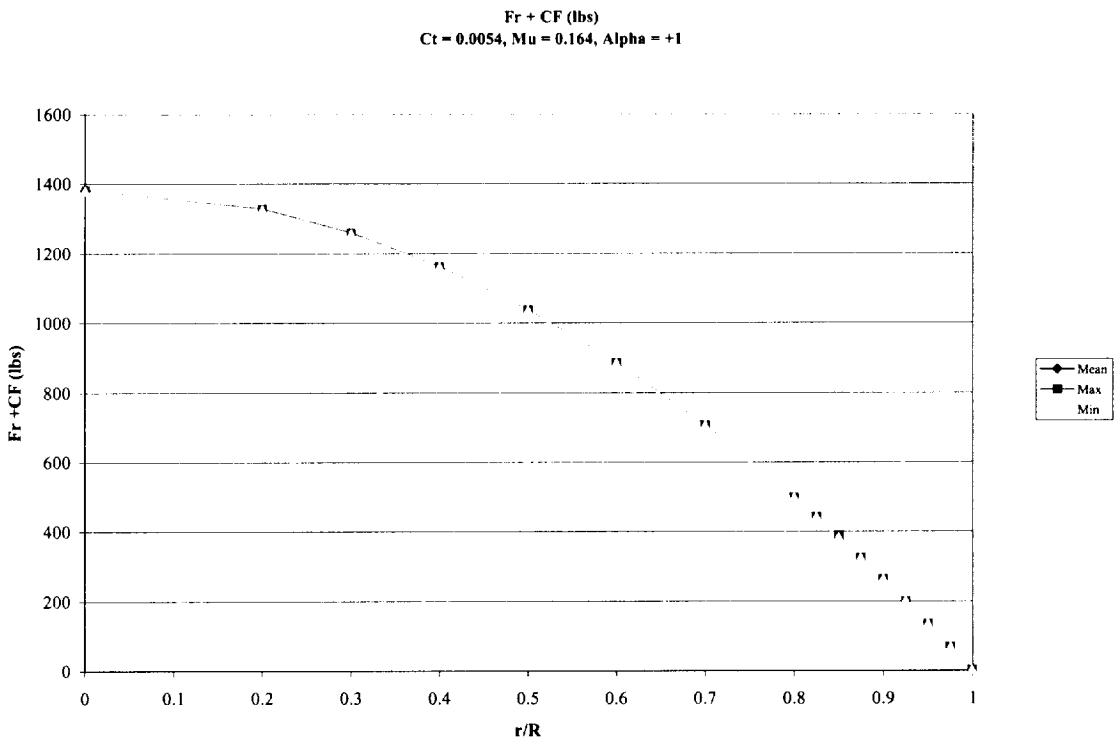


**Figure 17: Fr+CF vs. r/R**

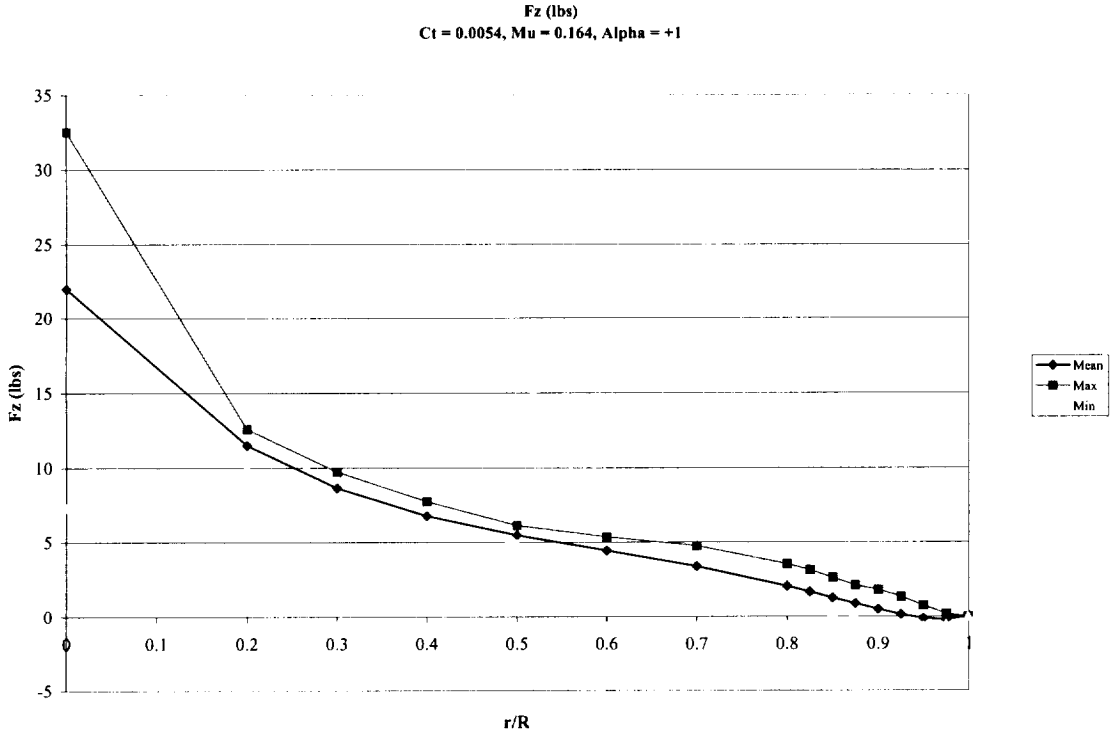


**Figure 18: Fz vs. r/R**

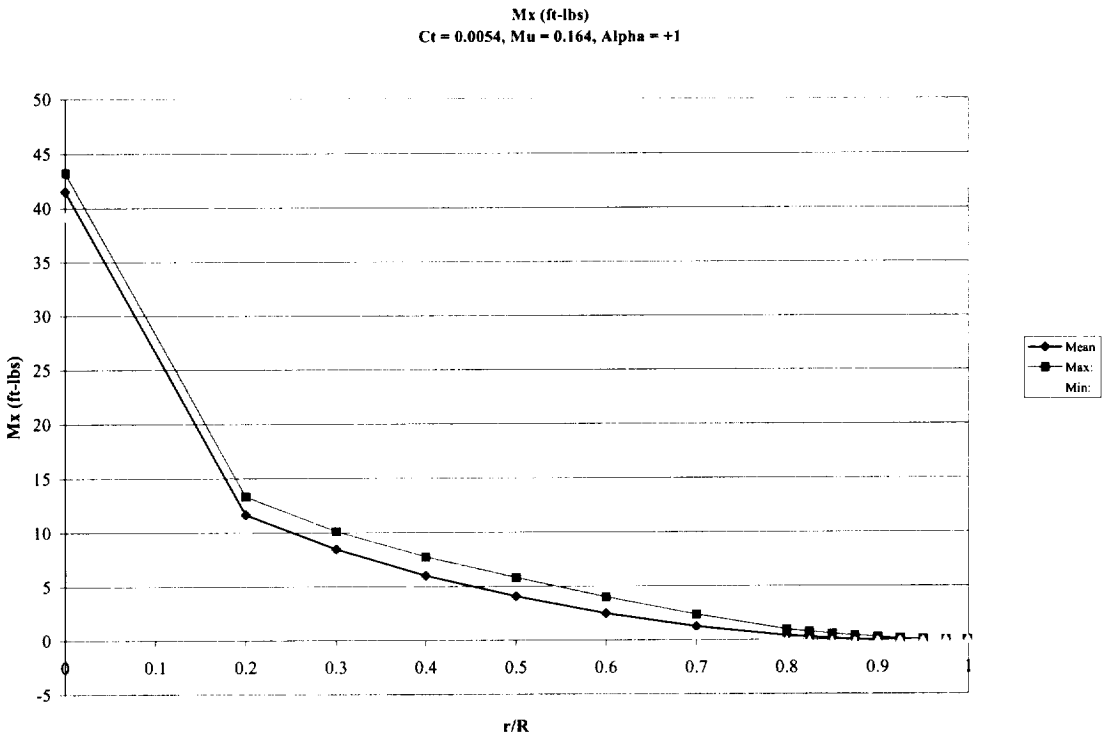


**Figure 19: Mx vs. r/R**

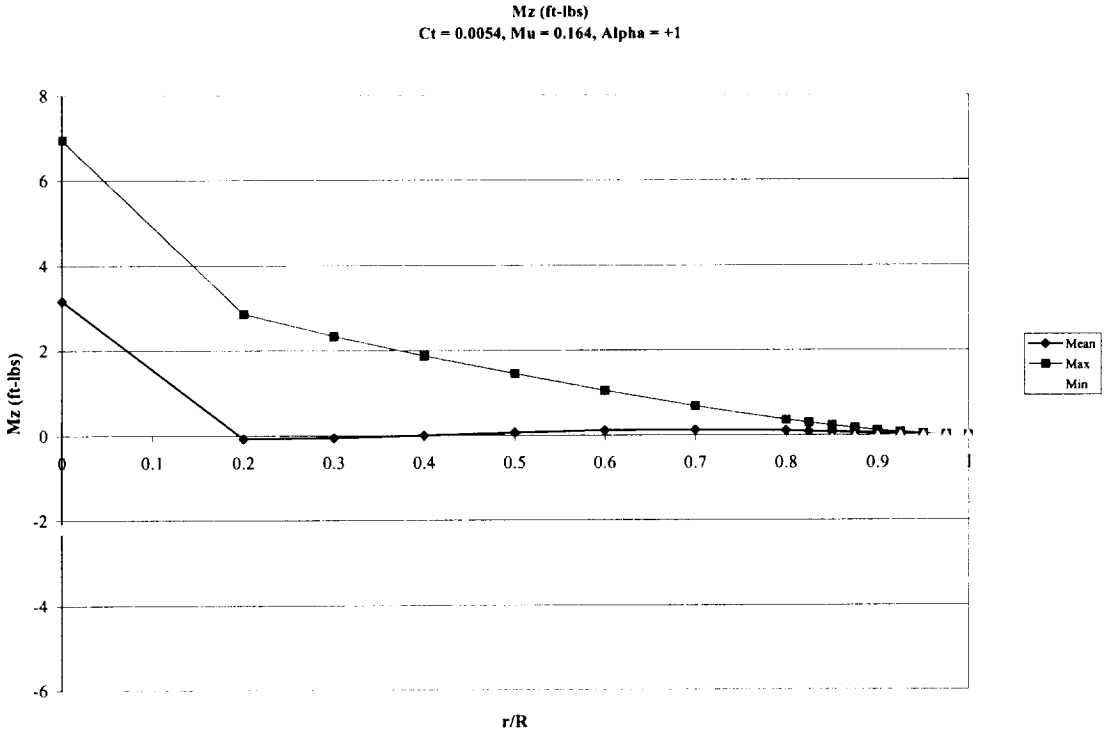


**Figure 20: Mz vs. r/R**

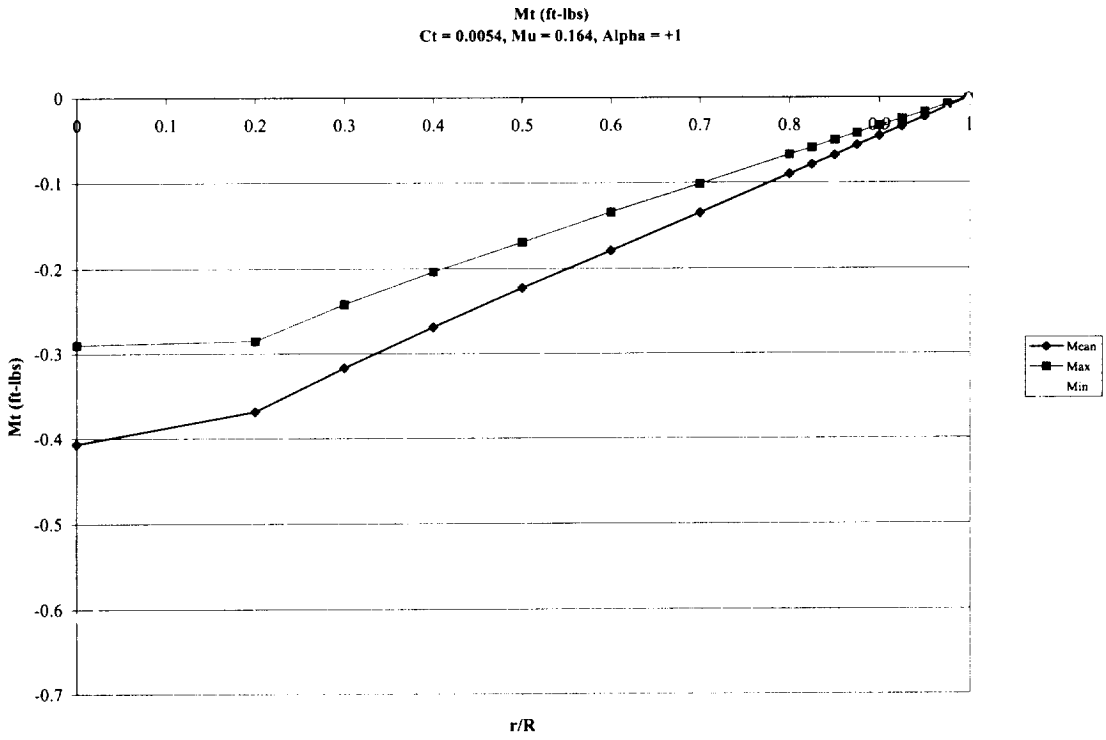


**Figure 21: Mt vs. r/R**

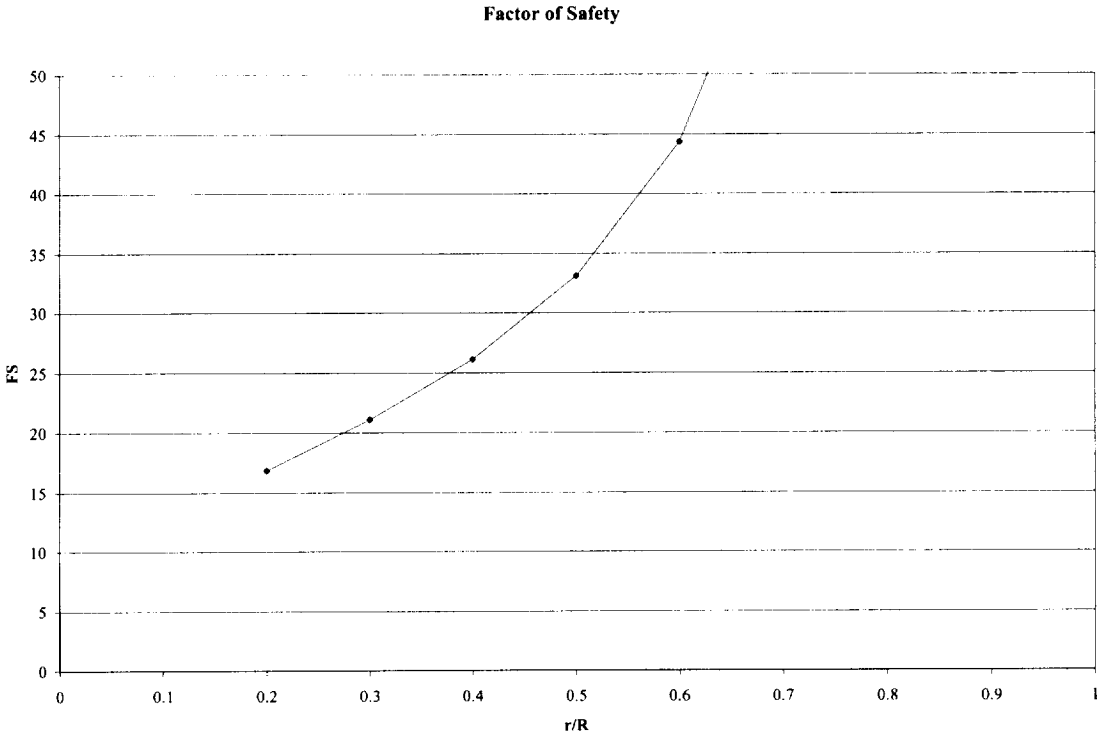


**Figure 22: Factor of Safety using Tsai-Hill Criteria vs. r/R**

## Conclusions

Computer simulation of the flip-tip rotor consisting of rotor free-wake model using the vortex-lattice method has shown that the concept has the potential to increase the miss distance between the rotor blades and their shed tip vortices. This increase in miss distance can lead to dramatic reduction in blade-vortex interaction noise. From the standpoint of the computer modeling, the concept seems to be a success. However, experimental testing of the concept is still needed and was to be a major portion of this study. Constraints on the use of the use of the 7' x 10' wind tunnel at NASA Ames prevented the tests from occurring and consequently, despite the favorable results from the computer model, judgment of the final success of the concept can not be made at this time.

## References


[1] Hardin, J. C. and Lampkin, S. L., "Concepts for Reduction of Blade/Vortex Interaction Noise." *Journal of Aircraft*, vol. 24, pp. 120-125, February 1987.

[2] Brooks, T. F., "Studies of Blade-Vortex Interaction Noise Reduction by Rotor Blade Modification." Presented at NOISE-CON 93, May 1993.

[3] Stroub, R. H., Young, L. A., Keys, C. N., and Cawthorne, M. H., "Free-Tip Rotor Wind Tunnel Test Results," *Journal of American Helicopter Society*, vol. 31, pp. 19-26, July 1986.

[4] P. Beaumier, *et al.*., "Effects of Higher Harmonic Control on Helicopter Rotor Blade-Vortex Interaction Noise: Prediction and Initial Validation." Presented at the AGARD Symposium on Aerodynamics and Aeroacoustics of Rotorcraft, October 1994.

[5] Kube, R., Splettstoesser, W. R., Wagner, W., Seelhorst, U., Yu, Y. H., Boutier, A., Micheli, F., and Mercker, E., "Initial Results from the Higher Harmonic Control Aeroacoustic Test (Hart) in the German-Dutch Wind Tunnel." Presented at the AGARD Symposium on Aerodynamics and Aeroacoustics of Rotorcraft, October 1994.

[6] Niesl, G., Swanson, S. M., Jacklin, S. A., Blaas, A., and Kube, R., "Effect of Individual Blade Control on Noise Radiation." Presented at the AGARD Symposium on Aerodynamics and Aeroacoustics of Rotorcraft, October 1994.

[7] Y. Yu, *et al.*., "Aerodynamics and Acoustics of Rotor Blade-Vortex Interactions: Analysis Capability and Its Validation," *AIAA-93-4332*, 1994.

[8] Gallman, J. M., Tung, C., Yu, Y., and Low, S. L., "Prediction of Blade-Vortex Interaction Noise with Applications to Higher Harmonic Control," *AIAA-93-4331*, 1993.

# Appendix A

Data on Forces and Moments for test rotor (baseline) from CAMRAD/JA.

| | FX (lbs) | | | | FR (lbs) | | | | FZ (lbs) | | | |
|---|---|---|---|---|---|---|---|---|---|---|---|---|
| r/R | Mean | Alt | Max | Min | Mean | Alt | Max | Min | Mean | Alt | Max | Min |
| 0 | 2.969 | 2.099 | 4.617 | 0.42 | -0.732 | 1.501 | 0.311 | -2.69 | 21.967 | 12.618 | 32.542 | 7.306 |
| 0.2 | 0.017 | 1.977 | 1.927 | -2.027 | -0.24 | 1.348 | 1.028 | -1.667 | 11.474 | 1.338 | 12.574 | 9.898 |
| 0.3 | -0.116 | 1.855 | 1.582 | -2.127 | -0.121 | 1.317 | 1.15 | -1.483 | 8.622 | 1.084 | 9.719 | 7.552 |
| 0.4 | -0.219 | 1.739 | 1.325 | -2.153 | -0.041 | 1.254 | 1.182 | -1.326 | 6.745 | 0.790 | 7.727 | 6.147 |
| 0.5 | -0.214 | 1.571 | 1.158 | -1.984 | 0.009 | 1.155 | 1.135 | -1.174 | 5.467 | 0.621 | 6.118 | 4.877 |
| 0.6 | -0.123 | 1.364 | 1.122 | -1.606 | 0.035 | 1.014 | 1.016 | -1.011 | 4.421 | 0.897 | 5.34 | 3.547 |
| 0.7 | -0.011 | 1.082 | 1.013 | -1.151 | 0.041 | 0.830 | 0.833 | -0.827 | 3.359 | 1.267 | 4.754 | 2.221 |
| 0.8 | 0.104 | 0.755 | 0.835 | -0.674 | 0.033 | 0.602 | 0.596 | -0.607 | 2.027 | 1.323 | 3.538 | 0.893 |
| 0.825 | 0.131 | 0.668 | 0.782 | -0.553 | 0.03 | 0.538 | 0.53 | -0.545 | 1.656 | 1.269 | 3.117 | 0.579 |
| 0.85 | 0.155 | 0.580 | 0.724 | -0.435 | 0.027 | 0.471 | 0.462 | -0.479 | 1.251 | 1.171 | 2.617 | 0.276 |
| 0.875 | 0.172 | 0.489 | 0.657 | -0.321 | 0.023 | 0.401 | 0.391 | -0.41 | 0.86 | 1.061 | 2.089 | -0.032 |
| 0.9 | 0.182 | 0.397 | 0.582 | -0.211 | 0.018 | 0.327 | 0.318 | -0.336 | 0.482 | 1.063 | 1.782 | -0.343 |
| 0.925 | 0.178 | 0.303 | 0.486 | -0.119 | 0.014 | 0.250 | 0.242 | -0.258 | 0.135 | 0.941 | 1.328 | -0.554 |
| 0.95 | 0.154 | 0.206 | 0.364 | -0.047 | 0.01 | 0.171 | 0.165 | -0.176 | -0.126 | 0.677 | 0.729 | -0.624 |
| 0.975 | 0.098 | 0.105 | 0.205 | -0.004 | 0.005 | 0.087 | 0.084 | -0.09 | -0.22 | 0.341 | 0.196 | -0.486 |
| 0.999 | 0.004 | 0.005 | 0.009 | 0 | 0 | 0.004 | 0.003 | -0.004 | -0.012 | 0.014 | 0.005 | -0.023 |

**Table 3: Cyclical loads predicted by CAMRAD/JA for the wind tunnel model (baseline case).**

| | MX (ft-lbs) | | | | MZ (ft-lbs) | | | | MT (ft-lbs) | | | |
|---|---|---|---|---|---|---|---|---|---|---|---|---|
| r/R | Mean | Alt | Max: | Min: | Mean | Alt | Max | Min | Mean | Alt | Max | Min |
| 0 | 41.509 | 2.038 | 43.257 | 39.182 | 3.158 | 4.578 | 6.953 | -2.203 | -0.407 | 0.160 | -0.29 | -0.609 |
| 0.2 | 11.662 | 1.607 | 13.352 | 10.138 | -0.076 | 3.363 | 2.857 | -3.869 | -0.369 | 0.121 | -0.285 | -0.526 |
| 0.3 | 8.464 | 1.542 | 10.125 | 7.041 | -0.058 | 2.717 | 2.331 | -3.102 | -0.317 | 0.103 | -0.242 | -0.448 |
| 0.4 | 6.019 | 1.621 | 7.787 | 4.545 | -0.005 | 2.103 | 1.871 | -2.334 | -0.269 | 0.087 | -0.204 | -0.378 |
| 0.5 | 4.068 | 1.563 | 5.812 | 2.687 | 0.06 | 1.529 | 1.454 | -1.603 | -0.223 | 0.073 | -0.169 | -0.314 |
| 0.6 | 2.479 | 1.335 | 4 | 1.331 | 0.109 | 1.016 | 1.055 | -0.976 | -0.179 | 0.059 | -0.134 | -0.252 |
| 0.7 | 1.243 | 0.965 | 2.364 | 0.435 | 0.121 | 0.591 | 0.681 | -0.5 | -0.135 | 0.045 | -0.101 | -0.191 |
| 0.8 | 0.369 | 0.536 | 0.991 | -0.08 | 0.099 | 0.273 | 0.362 | -0.183 | -0.09 | 0.031 | -0.067 | -0.128 |
| 0.825 | 0.248 | 0.439 | 0.752 | -0.125 | 0.087 | 0.209 | 0.289 | -0.129 | -0.079 | 0.027 | -0.059 | -0.112 |
| 0.85 | 0.106 | 0.372 | 0.55 | -0.193 | 0.077 | 0.154 | 0.227 | -0.081 | -0.068 | 0.024 | -0.05 | -0.097 |
| 0.875 | 0.022 | 0.295 | 0.386 | -0.203 | 0.063 | 0.107 | 0.168 | -0.045 | -0.056 | 0.020 | -0.042 | -0.081 |
| 0.9 | -0.004 | 0.206 | 0.255 | -0.157 | 0.044 | 0.072 | 0.114 | -0.03 | -0.045 | 0.016 | -0.033 | -0.065 |
| 0.925 | -0.034 | 0.123 | 0.12 | -0.126 | 0.03 | 0.041 | 0.069 | -0.012 | -0.034 | 0.012 | -0.025 | -0.049 |
| 0.95 | -0.035 | 0.055 | 0.033 | -0.077 | 0.016 | 0.018 | 0.033 | -0.003 | -0.023 | 0.008 | -0.017 | -0.033 |
| 0.975 | -0.016 | 0.013 | -0.001 | -0.027 | 0.005 | 0.005 | 0.009 | 0 | -0.011 | 0.004 | -0.008 | -0.016 |
| 0.999 | -0.001 | 0.000 | -0.001 | -0.001 | 0 | 0.000 | 0 | 0 | 0 | 0.001 | 0 | -0.001 |

**Table 4: Cyclical moments predicted by CAMRAD/JA for the wind tunnel model (baseline case).**